



HAL
open science

Impact of the Dynamic Electron Correlation on the Unusually Long Excited-State Lifetime of Thymine

Woojin Park, Seunghoon Lee, Miquel Huix-Rotllant, Michael Filatov, Cheol Ho Choi

► **To cite this version:**

Woojin Park, Seunghoon Lee, Miquel Huix-Rotllant, Michael Filatov, Cheol Ho Choi. Impact of the Dynamic Electron Correlation on the Unusually Long Excited-State Lifetime of Thymine. *Journal of Physical Chemistry Letters*, 2021, 12 (18), pp.4339-4346. 10.1021/acs.jpcllett.1c00712 . hal-03247474

HAL Id: hal-03247474

<https://amu.hal.science/hal-03247474>

Submitted on 19 Nov 2021

HAL is a multi-disciplinary open access archive for the deposit and dissemination of scientific research documents, whether they are published or not. The documents may come from teaching and research institutions in France or abroad, or from public or private research centers.

L'archive ouverte pluridisciplinaire **HAL**, est destinée au dépôt et à la diffusion de documents scientifiques de niveau recherche, publiés ou non, émanant des établissements d'enseignement et de recherche français ou étrangers, des laboratoires publics ou privés.

Impact of the Dynamic Electron Correlation on the Unusually Long Excited State Lifetime of Thymine

Woojin Park,[†] Seunghoon Lee,^{*,‡} Miquel Huix-Rotllant,^{*,¶} Michael Filatov,^{*,†} and Cheol Ho Choi^{*,†}

[†]*Department of Chemistry, Kyungpook National University, Daegu 702-701, South Korea*

[‡]*Division of Chemistry and Chemical Engineering, California Institute of Technology, Pasadena, California 91125, USA*

[¶]*Aix-Marseille Univ, CNRS, ICR, Marseille, France*

E-mail: slee89@caltech.edu; miquel.huixrotllant@univ-amu.fr; mike.filatov@gmail.com; cchoi@knu.ac.kr

Abstract

Relaxation of the photoexcited thymine in the gas-phase shows an unusually long excited-state lifetime, previously attributed to trapping in the absorbing excited state (S_2 -trapping mechanism). Here, we investigate this mechanism using the non-adiabatic molecular dynamics (NAMD) simulations combined with the recently developed Mixed Reference Spin-Flip (MRSF)-TDDFT method. We show that the S_2 -trapping was an artifact caused by an insufficient account of electron correlation in the electronic structure methodologies used for NAMD. The current work predicts instead an S_1 -trapping mechanism with two lifetimes, $\tau_1=30\pm 1$ fs and $\tau_2=6.1\pm 0.035$ ps, quantitatively consistent with time-resolved experiments. Upon excitation to S_2 ($\pi\pi^*$) state, thymine undergoes an ultrafast internal conversion from $S_2 \rightarrow S_1$ (*ca.* 30 fs) and resides

around the minimum on the S_1 ($n\pi^*$) surface slowly decaying to the ground state (*ca.* 6.1 ps). The $S_2 \rightarrow S_1$ internal conversion is mediated by bond length alternation stretching, which repeatedly passes through a newly found planar conical intersection region. The subsequent $S_1 \rightarrow S_0$ internal conversion occurs through several conical intersections involving slow puckering motions of the pyrimidine ring.

Keywords. Photochemistry, Molecular dynamics

Introduction

Photodynamics of nucleobases is of high interest given the potential solar UV damage inflicted on DNA and RNA. Experiments and theory established that nucleobases have a natural protection against this damage, thanks to several conical intersections, which, in their natural environment, efficiently release the energy and bring the nucleobases back to the ground state on an ultrafast timescale $\lesssim 1$ ps.^{1,2} In contrast, in the gas phase, many nucleobases display unusually long excited-state lifetimes on the order of several ps.³⁻¹³ In particular, thymine displays the longest gas phase decay constants, which are compiled in Table 1. The experimentally measured excited state dynamics of thymine can be split in three time domains: (i) an ultrafast step ($\lesssim 100$ fs),¹³ (ii) an intermediate step ($\sim 5-7$ ps), and (iii) a long relaxation (>1 ns) tail.³⁻¹² So far, theoretical simulations, also shown in Table 1, were unable to reproduce the experimental values with quantitative accuracy.

Theoretical simulations agree on the involvement of two excited states relevant for the internal conversion back to the S_0 state;^{21,22} namely, the optically bright S_2 state (characterized by a $\pi \rightarrow \pi^*$ orbital transition) and the dark S_1 state ($n \rightarrow \pi^*$ orbital transition). As regards the slow excited state decay kinetics of thymine, its mechanism still remains a subject of debate.^{3-12,14,23} Three different mechanisms of the internal conversion to S_0 were proposed based on the theoretical simulations of the photodynamics of thymine, as shown in Fig. 1. First, the S_1 -trapping model involves a sequential $\pi\pi^* \rightarrow n\pi^* \rightarrow S_0$ internal conversion, where the first step ($\pi\pi^* \rightarrow n\pi^*$) occurs on an ultrafast timescale¹³ and the second step ($n\pi^* \rightarrow S_0$) lasts for several picoseconds. Second, the S_2 -trapping model was proposed on the basis of the *ab initio* multiple spawning (AIMS)²³

Table 1: Experimental and theoretical excited-state lifetime constants of thymine in the gas phase under various pump and probe conditions. The experimental data were taken from compilation by Stojanović et al.¹⁴

Pump(nm)	Probe(nm)	τ_1 (fs)	τ_2 (ps)	τ_3 (ns)	Ref.
250	200	<50	0.49, 6.4		5
260	295	175	6.13	>1	3
266	2.19 (X-ray)	200-300			6
266	400/800	<100	7	long	7
266	800	200	7		8
267	2 x 400	105	5.12		9
267	800	100	7	>1	10
267	800		6.4	>100	4
270	193			293	11
272	800	130	6.5		12
	NEXAFS	60 ^{a)}	1.9, 10.5 ^{b)}	-	13
	MRSF - TDDFT	30±1 ^{c)}	6.1±0.035 ^{c)}	-	This work
	ADC(2)	~100 ^{d)} , 253 ^{e)}	0.391 ^{f)}	-	14
	CASSCF	100 ~ 200 ^{d)}	2.6 ~ 5 ^{e)}	-	2,15-17
	LR-TDDFT (PBE0 /SVP)	153 ^{a)}	13.9 ^{f)}	-	18
	Semiempirical (OM2/MRCI)	17 ^{a)}	0.42 ^{f)}	-	19

a) ($\pi\pi^* \rightarrow n\pi^*$) b) ($n\pi^* \rightarrow \text{non-}n\pi^*$) c) the margin of error is determined by bootstrapping²⁰ with 10^4 random samples. d) (FC \rightarrow S₂ min) e) (S₂ min \rightarrow S₁) f) ($n\pi^* \rightarrow$ S₀)

as well as the trajectory surface hopping (TSH) simulations based on the complete active space self-consistent field (CASSCF) potential energy surfaces (PES).^{2,15-17} In this model, the short time constant was explained by the relaxation of the S₂ state away from the Franck-Condon (FC) region towards a minimum on the S₂ surface where the molecule remains trapped for a long (*ca.* 5 ps) time.^{2,15-17} Finally, the S₂&S₁-trapping model was proposed based on quantum nuclear dynamics simulations,²⁴ where it was shown that a substantial redistribution of the population occurs between the S₂ and S₁ states during the first *ca.* 50 fs.

It should be underlined that the nonadiabatic molecular dynamics (NAMD) simulations, reported in the literature so far, were limited to a relatively short time domain, \lesssim 1 ps. The simulations performed at the CASSCF or the multireference configuration interaction with singles (MRCIS) levels typically neglect important parts of the dynamic electron correlation, which leads to large errors in the relative energies and the shapes of the excited state PESs.^{25,26} The dynamic electron

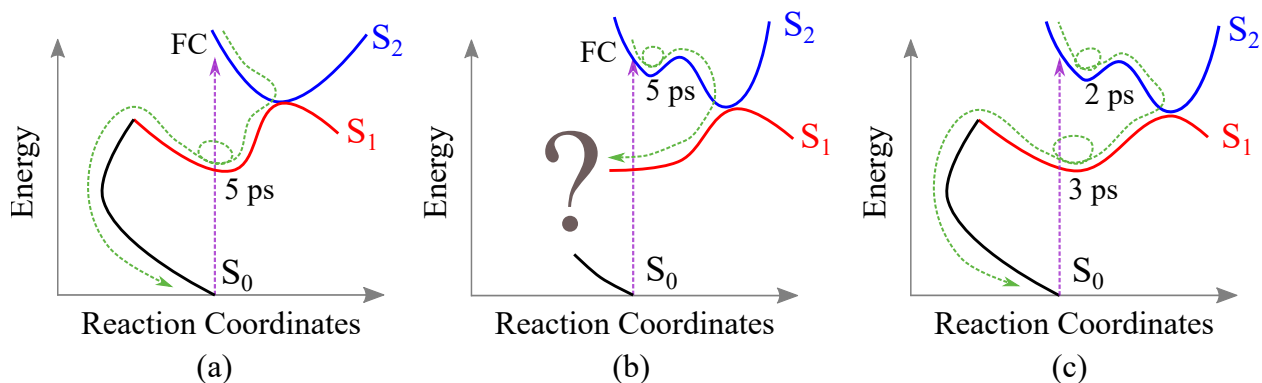


Figure 1: Previously proposed excited thymine decay pathways: (a) S_1 -trapping model, (b) S_2 -trapping model, and (c) S_1 & S_2 -trapping model.

correlation is essential for the correct description of the strength of chemical bonds as well as the vertical excitation energies; especially, when the excitation occurs in a state with (zwitter) ionic characteristics, such as the $\pi \rightarrow \pi^*$ state of thymine. Proper account of the dynamic correlation is a computationally demanding task, in particular, when the electronic states have pronounced multi-reference characteristics; *e.g.*, when chemical bonds are stretched or twisted far away from their equilibrium geometries.

None of the previous theoretical simulations capture all the experimentally observed aspects of the thymine photodynamics even at a qualitative level. Furthermore, the theoretical results display a marked dependence on the electronic structure method used in the simulations. Depending on the level of treatment of the dynamic electron correlation and multi-reference characteristics of the electronic states, the thymine NAMD simulations are biased to the S_2 -trapping or the S_1 -trapping mechanism. CASSCF and MRCIS methods, that essentially neglect the dynamic correlation, seem to favor the long S_2 lifetime, in contradiction with the experimental observation of a rapid $S_2 \rightarrow S_1$ decay.¹³ On the other hand, a shorter S_2 lifetime ($\tau_1 \sim 253$ fs) was obtained by Stojanović et al.¹⁴ who performed the NAMD simulations with the second-order algebraic-diagrammatic construction (ADC(2)) method where some dynamic correlation is taken into account. This seems to shift the balance towards the S_1 -trapping mechanism. However, ADC(2) is a single-reference method and it cannot describe the dimensionality of the S_1/S_0 conical intersection seam in a proper way.²⁷ Thus, the ADC(2) NAMD simulations¹⁴ produced a very short S_1 state lifetime $\tau_2 \sim 391$ fs, which is not

compatible with the experimental observations either. A similar, albeit not identical, lifetimes were obtained in the LR-TDDFT (linear-response time-dependent DFT) simulations by Parker et al.,¹⁸ see Table 1. However, LR-TDDFT suffers from the same drawbacks (the inability to properly describe the S_1/S_0 conical intersections and the lack of the multi-reference effects in the ground state) as the ADC(2) method. Hence, these simulations failed to produce the critical evidence in favor of either decay mechanism. Thus, to obtain a definitive answer it is necessary to perform theoretical simulations using a methodology that: (i) provides for a balanced and accurate account of both the dynamic correlation as well as the multi-reference characteristics of the electronic states, (ii) , is capable of correctly describing the conical intersections between the ground and excited electronic states, and (iii) is efficient enough to perform statistical dynamical samplings for several picoseconds .

In the present work, we employ the recently developed mixed-reference spin-flip time-dependent density functional theory (MRSF-TDDFT; MRSF, for brevity)²⁸ method, which enables fast and accurate computation of the ground and excited electronic states with the inclusion of the dynamic correlation and the multi-reference characteristics. An important advantage of MRSF before the usual linear-response TDDFT^{29–31} is that MRSF enables proper computation of the S_1/S_0 conical intersections;³² which is crucial for the accurate description of the dynamics of the excited states.

Results and Discussion

Vertical excitation energies of thymine. The MRSF /B3LYP computations of the vertical excitation energies (VEE) to the optically bright S_2 (the $\pi \rightarrow \pi^*$ transition) are in an excellent agreement (*ca.* 0.1 eV) with the experiments and perturbation theories of ADC(2) and MS-CASPT2. On the other hand, the corresponding values of both MRSF and LR-TDDFT with BH&HLYP XC functionals, become closer to high level computational approaches of MRCISD+Q and EOM-CCSD within *ca.* 0.3 eV. (See Table ??).²⁵ As was pointed out by Huix-Rotllant et al.,³³ within the widely used collinear (one-component) SF formalism, the configurations obtained by different SF transitions

couple through the exact exchange only. As the current implementation of MRSF also utilizes the collinear formalism, it was shown that MRSF requires more exact exchange contribution (such as BHLYP).³⁴ Therefore, all the calculations were carried out using the BH&HLYP. The effect of B3LYP on dynamics shall be also discussed later. The S_0 equilibrium geometry of thymine obtained with MRSF/BH&HLYP is in an excellent agreement with the experimental crystallographic geometry; see the Fig. ??.

The nonadiabatic molecular dynamics (NAMD) Simulations. The TSH NAMD simulations with MRSF/BH&HLYP are initiated in the bright S_2 state by sampling the S_0 Wigner distribution at $T = 300\text{K}$; see the Supporting Information for more detail. One hundred trajectories were propagated up to 2 ps; 89 trajectories out of one hundred have finished successfully and are used for the analysis in the following.

Fig. 2 (a) and (b) show the time evolution of the populations of the S_2 , S_1 , and S_0 adiabatic states. Within the first *ca.* 50 fs, the population of the S_2 state drops below 0.3 due to the $S_2 \rightarrow S_1$ ($\pi\pi^* \rightarrow n_O\pi^*$) population transfer. This result is in a good agreement with the experimental observations reported by Wolf et al.¹³ ($\tau_{\pi\pi^* \rightarrow n\pi^*} = 60 \pm 30$ fs). At longer times, $t \gtrsim 100$ fs, almost all of the S_2 population ends up in the S_1 state, where it slowly decays in the S_0 state. The exponential decay parameter obtained by fitting the S_1 population decay by a mono-exponential function is *ca.* 6.1 ps, which is in a qualitative agreement with the experimental estimates of 5–7 ps; see Table 1. Hence, the TSH NAMD simulations with MRSF/BH&HLYP clearly support the S_1 trapping mechanism.

At the early simulation times, $t \lesssim 50$ fs, the pyrimidine ring remains planar and the major geometric changes involve elongation of the $C_4=O_8$ and $C_5=C_6$ double bonds and shortening of the C_4-C_5 single bond (See Fig. 2(d) for the atom numbering). This leads to bond length alternation (BLA) in the pyrimidine ring. The so-defined BLA parameter characterizes the magnitude of the geometric distortion away from the FC region and its time evolution, as shown in Fig. 2(c). During the first *ca.* 20–30 fs, there is a pronounced synchronicity of the BLA distortion among

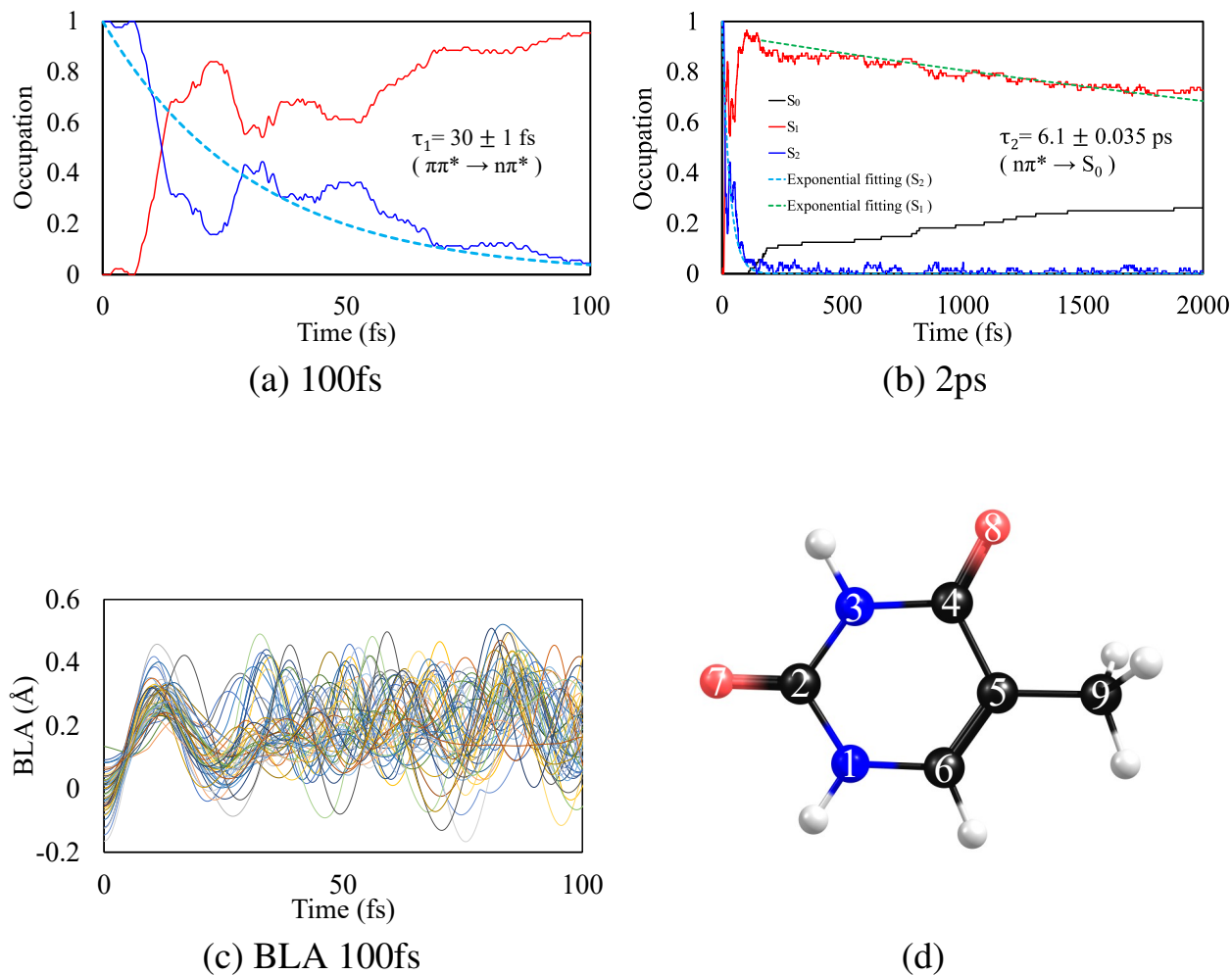


Figure 2: Time evolution of the adiabatic S_0 , S_1 , and S_2 populations for (a) the first 100 fs and (b) the entire 2 ps duration of the NAMD simulations. The NAMD simulations were performed up to 2000 fs with a time-step 0.5 fs for propagation of the nuclear degrees of freedom. The initial geometries were generated by sampling the Wigner distribution at $T=300\text{K}$; see the text for more detail. The light blue curve in the panel (a) and the green curve in the panel (b) represent fittings of the S_2 and S_1 populations by a mono-exponential function respectively. Panel (c) shows the time evolution of bond length alternation (BLA) along the trajectories within the first 100 fs of the simulation. The BLA coordinate is defined here as the difference between the average increments of the lengths of the double bonds and the decrease of the single bond, $\text{BLA} = \frac{1}{2}(\Delta R_{\text{C}_4=\text{O}_8} + \Delta R_{\text{C}_5=\text{C}_6}) - \Delta R_{\text{C}_4-\text{C}_5}$, where ΔR 's are displacements with respect to the S_0 equilibrium geometry. (d) The atom numbering of thymine.

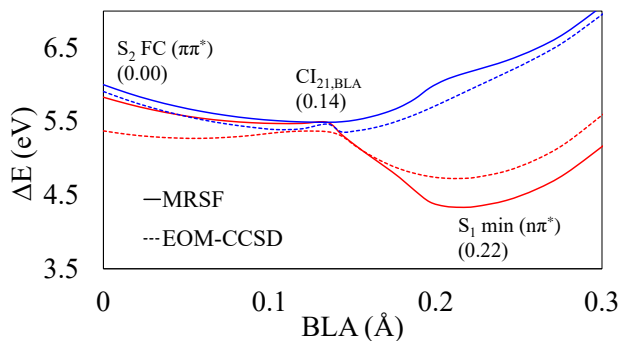
all the trajectories. This suggests that a concerted displacement along the BLA coordinate causes an ultrafast transfer of the S_2 population to S_1 ; see Fig. 2(a). The synchronicity is rapidly lost, becoming incoherent after *ca.* 50 fs.

The decay to the S_0 state requires reaching one of the S_1/S_0 CIs, most of which involve puckering of the pyrimidine ring, see Fig. ???. In total, 23 trajectories ended up in the S_0 state after 2 ps. The lowest S_1/S_0 minimum energy crossing point (MECP) is located 5.8 kcal/mol above the minimum on the adiabatic S_1 PES, see $CI_{10,A}$ in Fig. ???. The other S_1/S_0 MECs, $CI_{10,B}$, $CI_{10,C}$, and $CI_{10,D}$ in Fig. ??? occur at higher relative energies, *ca.* 20–30 kcal/mol. Although these CIs lie below the vertical excitation energy at the FC geometry, reaching them requires strong puckering of the pyrimidine ring accompanied by bending of the extra-cyclic groups. Together with the energy barrier to reach the S_1/S_0 CI seam, the poor accessibility of the S_1/S_0 seam causes trapping of the trajectories in the S_1 minimum. In this regard, the present TSH NAMD simulations definitively support the S_1 trapping model.

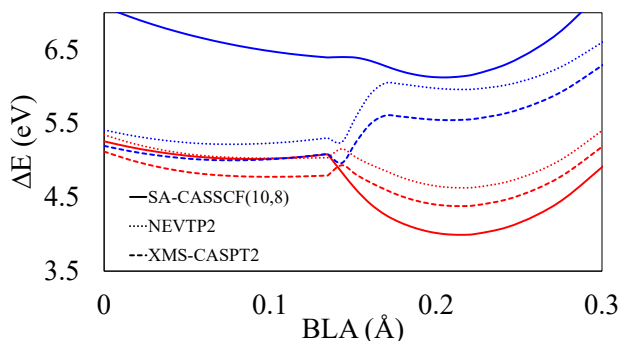
The ultrafast decay of the S_2 population at the early times is rather peculiar and deserves further discussion. In the previous theoretical simulations of the thymine photodynamics,^{14,15,23} the $S_2 \rightarrow S_1$ decay was assigned to occur through a puckered S_2/S_1 CI, $CI_{21,\phi}$ in Fig. ??? (ϕ is defined as the $N_1C_6C_5C_9$ dihedral angle; see Fig. 2(d)). As reaching this CI involves puckering of the pyrimidine ring, which is a relatively slow motion, this decay mechanism is incompatible with the ultrafast $S_2 \rightarrow S_1$ decay observed in our TSH NAMD simulations as well as measured experimentally.¹³ Starting from the snapshots of our NAMD trajectories at which the $S_2 \rightarrow S_1$ surface hops occur, a new S_2/S_1 CI was located, which features planar pyrimidine ring geometry and can be reached from the FC region by the BLA distortion; see $CI_{21,BLA}$ in Fig. ???.

Comparison with the *ab initio* methods. Using the MRSF/BH&HLYP optimized geometries of the FC region, $CI_{21,BLA}$, and $S_{1,min}$, all of which are planar, a minimum energy path (MEP) was constructed on the S_2 and S_1 PESs by the nudged elastic band (NEB) method.^{38,39} In Figs. 3(a), (b), and (c), the S_2 and S_1 PES profiles along the MEP are shown; the MEP is characterized by the BLA distortion. The MRSF results are compared with the PES profiles obtained along the same MEP by other theoretical methods.

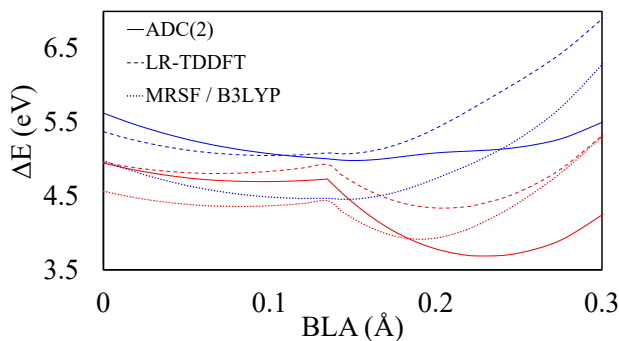
Inferred from MRSF results, the S_2 and S_1 PESs undergo a crossing at BLA value of 0.14 Å and



(a)



(b)



(c)

Figure 3: MEPs on the S_2 and S_1 PESs optimized using the NEB method in connection with MRSF and connecting the FC region, the $CI_{21,BLA}$, and the $S_{1,min}$ geometries; the respective BLA values are given parenthetically. For all other electronic structure methods, the MRSF MEP geometries are obtained employing a 6-31G* basis set and Cs symmetry restriction. Panel (a) compares the S_2 (blue) and S_1 (red) PES profiles along the MRSF MEPs (solid lines) with the EOM-CCSD curves (dashed lines). Panel (b) shows the S_2 and S_1 PES profiles obtained with the SA-CASSCF(10,8) (solid lines), the eXtended Multi-State Complete Active Space second-order Perturbation Theory (XMS-CASPT2, dashed lines), and the n-electron valence state perturbation theory (NEVPT2, dotted lines). Panel (c) shows the S_2 and S_1 PES profiles obtained with the ADC(2) (solid lines), LR-TDDFT / PBE0 (dashed lines), and MRSF / B3LYP (dotted lines). The results of MRSF, EOM-CCSD, and LR-TDDFT were obtained with GAMESS,³⁵ ADC(2) with TURBOMOLE,³⁶ while the rests were obtained with Molpro.³⁷

then the S_1 PES rapidly descends to the $S_{1,min}$ geometry at $BLA = 0.22 \text{ \AA}$. The MRSF curves (solid curves) are in a good qualitative agreement with the EOM-CCSD/6-31G* method (dashed curves); see also Fig. ?? for the EOM-CCSD calculations with a bigger basis set. As the S_2 ($\pi\pi^*$) and S_1 ($n\pi^*$) states have different symmetry, the intersection is allowed and the EOM-CC formalism does not produce any artifacts.⁴⁰ Although EOM-CCSD is a single-reference methodology, its application along the BLA path is justified as confirmed by the T_1 diagnostics shown in Fig. ?. The NEVPT2 and the XMS-CASPT2 methods are multi-reference methodologies, which do not suffer from possible artifacts inherent in single-reference methods, such as EOM-CC, ADC(2), or LR-TDDFT. Both methods include the dynamic electron correlation and the S_2 and S_1 potential energy profiles produced by these methods along the BLA path in Fig. 3b show very similar shapes to the MRSF profiles. A positive match with the energy profiles produced by the high-level correlated methods helps to establish the correctness of the PES profiles obtained with MRSF/BH&HLYP; hence, of the entire deactivation reaction mechanism deduced from the MRSF/BH&HLYP TSH-NAMD simulations.

In Fig. 3(b), the curves obtained using the CASSCF (solid lines) are compared with the NEVPT2 (dotted lines), and the XMS-CASPT2 (dashed lines) curves. Distinctively, the CASSCF method, which neglects the dynamic electron correlation, does not predict a crossing between the S_2 and S_1 states along the BLA path. Instead, it predicts a shallow minimum on the S_2 PES, which is separated by more than 2 eV from the minimum on the S_1 PES. In the CASSCF picture, the $S_2 \rightarrow S_1$ population transfer is only possible due to a pronounced puckering distortion of the pyrimidine ring ($CI_{21,\phi}$),^{2,15,23} which results in a slow $\pi\pi^* \rightarrow n\pi^*$ relaxation time and supports the S_2 -trapping model. Therefore, the lack of the dynamic electron correlation in CASSCF destabilizes the $\pi\pi^*$ (S_2) state relative to the $n\pi^*$ (S_1) state and leads to the absence of the S_2/S_1 crossing along the BLA path. In fact, the overestimation of the energy of the $\pi\pi^*$ states by CASSCF was also observed in a series of polyenes,⁴¹ where the inclusion of the dynamic correlation considerably improves the vertical excitation energies of these states. Hence, it can be confidently concluded that the lack of dynamic electron correlation in CASSCF leads to an erroneous prediction of the S_2 -trapping at the

origin of the long excited lifetime of thymine.

In Fig. 3(c), the curves obtained using the ADC(2) (solid lines), the LR-TDDFT (dashed lines) and MRSF/B3LYP (dotted lines) methods are shown. It is noteworthy that ADC(2), used by Stojanović et al.¹⁴ in their NAMD simulations, yields a gap of *ca.* 0.30 eV (0.1 eV with a larger def2-QZVP basis set in Fig. ??) between the S_2 and S_1 states, at the geometry where the other correlated methods predict an S_2/S_1 crossing. This demonstrates that ADC(2) provides only a partial account of the dynamic correlation; mainly due to a slow convergence of the perturbation theory to the exact result. Hence, the NAMD simulations of Stojanović et al.¹⁴ yield a much too long $S_2 \rightarrow S_1$ relaxation time (*ca.* 253 fs; see Table 1) inconsistent with the experiment (60 ± 30 fs).¹³

Similarly, the LR-TDDFT/PBE0/SVD curves in Fig. 3(c) feature a gap of *ca.* 0.15 eV. The LR-TDDFT/PBE0/SVD method was used by Parker et al.¹⁸ in their NAMD simulations which yielded 153 fs for the $S_2 \rightarrow S_1$ relaxation time. Hence, there seems to be correlation between the S_2/S_1 gap along the BLA path and the predicted $S_2 \rightarrow S_1$ relaxation time: CASSCF – 1.5 eV and ~ 5 ps, ADC(2) – 0.3 eV and 253 fs,¹⁴ LR-TDDFT – 0.15 eV and 153 fs,¹⁸ MRSF – 0 eV and ~ 30 fs. It may therefore be conjectured that the other computational methods, *e.g.* XMS-CASPT2 or NEVPT2, which yield the qualitatively correct S_2 and S_1 surfaces, should predict equally short $S_2 \rightarrow S_1$ relaxation time. Likewise, the zero gap by MRSF/B3LYP (dotted line) in 3(c) also implies a short time.

As already mentioned in the introduction, an important difference between the MRSF method used here (also the multi-reference methods, such as XMS-CASPT2, or NEVPT2) and the single-reference methodologies, such as ADC(2) and LR-TDDFT, is that the latter methodologies are incapable of describing the correct double cone topology of the S_1/S_0 conical intersections.^{27,42,43} Instead, ADC(2) and LR-TDDFT yield a linear (not conical) crossing between these states.^{27,42,43} As a linear crossing seam has a greater dimension than a true conical intersection, this leads to an incorrect description of the $S_1 \rightarrow S_0$ non-adiabatic population transfer.⁴² Certain artifacts are also produced by the full-response LR-TDDFT method for the symmetry forbidden intersections

between the excited states, which lack the proper double cone topology.⁴⁰ Hence, the predictions of the single-reference methodologies, ADC(2) and LR-TDDFT, lack reliability in describing the non-adiabatic relaxation of the excited states. The MRSF method on the other hand is perfectly capable of describing the correct topology of the conical intersections³² and it yields the energy of the mechanistically important S_1/S_0 CIs in a good agreement with the correlated multi-reference methodologies; see Fig. ?? for comparison with the NEVPT2 method. This reaffirms the validity and the reliability of the results obtained in this work for the mechanism of thymine deactivation.

Conclusions

The results of our NAMD simulations by MRSF and the investigation of the S_2 , S_1 , and S_0 adiabatic PESs provide decisive evidence supporting the S_1 -trapping mechanism of excited thymine relaxation in the gas phase. The MEPs in Fig. 4 constructed using the stationary points and conical intersections illustrate the main results of the present work. Upon excitation in the S_2 ($\pi\pi^*$) state, thymine rapidly (*ca.* 30 fs) undergoes an ultrafast non-adiabatic population transfer in the S_1 ($n\pi^*$) state, where it resides for a long time (*ca.* 6.1 ps) inside a minimum on the S_1 PES. The $S_2 \rightarrow S_1$ population transfer is mediated by a very fast internal BLA motion, which involves the $C_4=O_8$ and $C_5=C_6$ double bonds and the C_4-C_5 single bond of the pyrimidine ring and repeatedly passes through $CI_{21,BLA}$; the latter CI was identified in this work for the first time. The rapid $\pi\pi^* \rightarrow n\pi^*$ internal conversion is supported by the experimental evidence, where an ultrafast relaxation occurs with a decay constant of 60 ± 30 fs.¹³ The subsequent $S_1 \rightarrow S_0$ population transfer occurs through several S_1/S_0 conical intersections, which involve puckering of the pyrimidine ring (see Fig. ?? for geometries); the two predominantly visited CIs are shown in Fig. 4 and they occur *ca.* 1.00 eV ($CI_{10,B}$) and 1.53 eV ($CI_{10,C}$) above the bottom of the S_1 minimum. Although both CIs occur below the S_2 vertical excitation energy (6.00 eV), the probability of reaching them is fairly low, as it requires a substantial geometric distortion.

From the obtained results, a conclusion can be drawn that the previously proposed S_2 -trapping

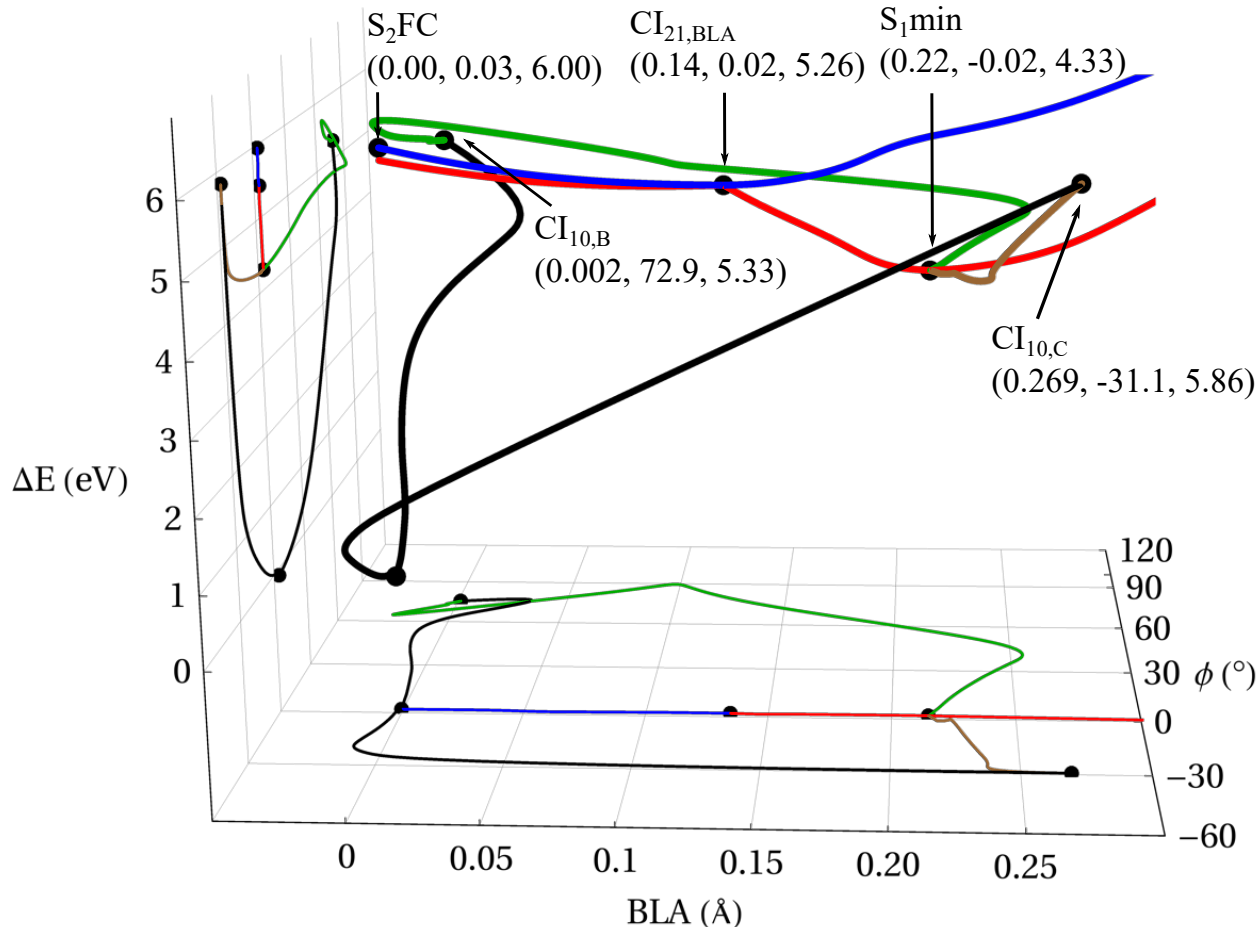


Figure 4: In addition to the profiles of potential energy surface(PES) connecting FC – $CI_{21,BLA}$ – $S_{1,min}$ along the BLA coordinate of Fig. 3, the MEPs of $S_{1,min}$ – $CI_{10,B}$ and $S_{1,min}$ – $CI_{10,C}$ are obtained by the nudged elastic band.^{38,39} Using these, the 3D plot of minimum energy pathways along photo-excited thymine deactivation pathways to ground S_0 state are constructed, where two major coordinates of the BLA and ϕ ($= N_1C_6C_5C_9$) are adopted. The blue(S_2) and red(S_1) curves are along S_2FC – $CI_{21,BLA}$ – $S_{1,min}$, representing the faster dynamics between S_2 and S_1 . The two major channels from S_1 to S_0 state are the green ($S_{1,min}$ – $CI_{10,B}$) and brown ($S_{1,min}$ – $CI_{10,C}$). The S_0 is in black curve. The values in the parenthesis are BLA, ϕ and relative energy in eV.

mechanism is caused by an insufficient account of the dynamic electron correlation in the computational methodologies (CASSCF and MRCIS) used in the NAMD simulations. Due to the absence of the dynamic correlation, the CASSCF method does not yield an S_2/S_1 conical intersection in the vicinity of the FC region and, therefore, the NAMD trajectories are trapped in a local minimum on the S_2 PES. The proper account of the dynamic correlation corrects this deficiency and recovers an ultrafast S_2/S_1 internal conversion measured experimentally;¹³ thus, resolving the long-standing

controversy. As the NAMD simulations performed with the CASSCF electronic structure method pervade the literature on the excited state dynamics, the results of this work suggest that many conclusions drawn from these simulations may need to be reassessed. Besides providing a reliable computational evidence in favor of the S_1 -trapping mechanism of the internal conversion of excited thymine, the present work establishes the MRSF methodology as an accurate computational tool capable of predicting molecular photophysics in close agreement with the experiment.

Acknowledgement

This work was supported by the Samsung Science and Technology Foundation (SSTF-BA1701-12)

Supporting Information

A separate supporting information file is provided.

References

- (1) Pecourt, J.-M. L.; Peon, J.; Kohler, B. *J. Am. Chem. Soc.* **2000**, *122*, 9348–9349.
- (2) Barbatti, M.; Aquino, A. J.; Szymczak, J. J.; Nachtigallová, D.; Hobza, P.; Lischka, H. *Proc. Natl. Acad. Sci. U.S.A* **2010**, *107*, 21453–21458.
- (3) Yu, H.; Sanchez-Rodriguez, J. A.; Pollum, M.; Crespo-Hernández, C. E.; Mai, S.; Marquetand, P.; González, L.; Ullrich, S. *Phys. Chem. Chem. Phys.* **2016**, *18*, 20168–20176.
- (4) Kang, H.; Lee, K. T.; Jung, B.; Ko, Y. J.; Kim, S. K. *J. Am. Chem. Soc.* **2002**, *124*, 12958–12959.
- (5) Ullrich, S.; Schultz, T.; Zgierski, M. Z.; Stolow, A. *Phys. Chem. Chem. Phys.* **2004**, *6*, 2796–2801.
- (6) McFarland, B. K. et al. *Nat. Commun.* **2014**, *5*, 4235.
- (7) González-Vázquez, J.; González, L.; Samoylova, E.; Schultz, T. *Phys. Chem. Chem. Phys.* **2009**, *11*, 3927–3934.
- (8) Gador, N.; Samoylova, E.; Smith, V. R.; Stolow, A.; Rayner, D. M.; Radloff, W.; Hertel, I. V.; Schultz, T. *J. Phys. Chem. A* **2007**, *111*, 11743–11749.
- (9) Canuel, C.; Mons, M.; Piuze, F.; Tardivel, B.; Dimicoli, I.; Elhanine, M. *J. Chem. Phys.* **2005**, *122*, 074316.
- (10) Samoylova, E.; Schultz, T.; Hertel, I. V.; Radloff, W. *Chem. Phys.* **2008**, *347*, 376–382.
- (11) Ligare, M.; Siouri, F.; Bludsky, O.; Nachtigallová, D.; de Vries, M. S. *Phys. Chem. Chem. Phys.* **2015**, *17*, 24336–24341.
- (12) Samoylova, E.; Lippert, H.; Ullrich, S.; Hertel, I. V.; Radloff, W.; Schultz, T. *J. Am. Chem. Soc.* **2005**, *127*, 1782–1786.

- (13) Wolf, T. J. A. et al. *Nat. Commun.* **2017**, *8*, 29.
- (14) Stojanović, L.; Bai, S.; Nagesh, J.; Izmaylov, A.; Crespo-Otero, R.; Lischka, H.; Barbatti, M. *Molecules* **2016**, *21*, 1603.
- (15) Szymczak, J. J.; Barbatti, M.; Soo Hoo, J. T.; Adkins, J. A.; Windus, T. L.; Nachtigallová, D.; Lischka, H. *J. Phys. Chem. A* **2009**, *113*, 12686–12693.
- (16) Asturiol, D.; Lasorne, B.; Worth, G. A.; Robb, M. A.; Blancafort, L. *Phys. Chem. Chem. Phys.* **2010**, *12*, 4949–4958.
- (17) Picconi, D.; Barone, V.; Lami, A.; Santoro, F.; Improta, R. *ChemPhysChem* **2011**, *12*, 1957–1968.
- (18) Parker, S. M.; Roy, S.; Furche, F. *Phys. Chem. Chem. Phys.* **2019**, *21*, 18999–19010.
- (19) Lan, Z.; Fabiano, E.; Thiel, W. *The Journal of Physical Chemistry B* **2009**, *113*, 3548–3555.
- (20) Nangia, S.; Jasper, A. W.; Miller, T. F.; Truhlar, D. G. *J. Chem. Phys.* **2004**, *120*, 3586–3597.
- (21) Yamazaki, S.; Taketsugu, T. *J. Phys. Chem. A* **2012**, *116*, 491–503.
- (22) Perun, S.; Sobolewski, A. L.; Domcke, W. *J. Phys. Chem. A* **2006**, *110*, 13238–13244.
- (23) Hudock, H. R.; Levine, B. G.; Thompson, A. L.; Satzger, H.; Townsend, D.; Gador, N.; Ullrich, S.; Stolow, A.; Martinez, T. J. *J. Phys. Chem. A* **2007**, *111*, 8500–8508.
- (24) Picconi, D.; Barone, V.; Lami, A.; Santoro, F.; Improta, R. *ChemPhysChem* **2011**, *12*, 1957–1968.
- (25) Zechmann, G.; Barbatti, M. *J. Phys. Chem. A* **2008**, *112*, 8273–8279.
- (26) Asturiol, D.; Lasorne, B.; Robb, M. A.; Blancafort, L. *J. Phys. Chem. A* **2009**, *113*, 10211–10218.

- (27) Tuna, D.; Lefrancois, D.; Wolański, Ł.; Gozem, S.; Schapiro, I.; Andruniów, T.; Dreuw, A.; Olivucci, M. *J. Chem. Theory Comput.* **2015**, *11*, 5758–5781.
- (28) Lee, S.; Filatov, M.; Lee, S.; Choi, C. H. *J. Chem. Phys.* **2018**, *149*, 104101.
- (29) Casida, M. E.; Jamorski, C.; Bohr, F.; Guan, J.; Salahub, D. R. *Optical properties from density-functional theory*; ACS Publications, 1996.
- (30) Fiolhais, C.; Nogueira, F.; Marques, M. A. *A primer in density functional theory*; Springer Science & Business Media, 2003; Vol. 620.
- (31) Casida, M. E.; Huix-Rotllant, M. *Annu. Rev. Phys. Chem.* **2012**, *63*, 287–323.
- (32) Lee, S.; Shostak, S.; Filatov, M.; Choi, C. H. *J. Phys. Chem. A* **2019**, *123*, 6455.
- (33) Huix-Rotllant, M.; Natarajan, B.; Ipatov, A.; Wawire, C. M.; Deutsch, T.; Casida, M. E. *Phys. Chem. Chem. Phys.* **2010**, *12*, 12811–12825.
- (34) Horbatenko, Y.; Lee, S.; Filatov, M.; Choi, C. H. *J. Phys. Chem. A* **2019**, *123*, 7991–8000.
- (35) Schmidt, M. W.; Baldridge, K. K.; Boatz, J. A.; Elbert, S. T.; Gordon, M. S.; Jensen, J. H.; Koseki, S.; Matsunaga, N.; Nguyen, K. A.; Su, S.; Windus, T. L.; Dupuis, M.; Montgomery Jr, J. A. *J. Comput. Chem* **1993**, *14*, 1347–1363.
- (36) TURBOMOLE V7.1 2016, a development of University of Karlsruhe and Forschungszentrum Karlsruhe GmbH, 1989-2007, TURBOMOLE GmbH, since 2007; available from <http://www.turbomole.com>.
- (37) Werner, H.-J.; Knowles, P. J.; Knizia, G.; Manby, F. R.; Schütz, M. *Wiley Interdisciplinary Reviews: Computational Molecular Science* **2012**, *2*, 242–253.

- (38) Jónsson, H.; Mills, G.; Jacobsen, K. W. In *Classical and Quantum Dynamics in Condensed Phase Simulations*; Berne, B. J., Ciccotti, G., Coker, D. F., Eds.; World Scientific: Singapore, 1998; Chapter 16, pp 385–404.
- (39) Kästner, J.; Carr, J. M.; Keal, T. W.; Thiel, W.; Wander, A.; Sherwood, P. J. *Phys. Chem. A* **2009**, *113*, 11856–11865.
- (40) Kjørstad, E. F.; Myhre, R. H.; Martínez, T. J.; Koch, H. *J. Chem. Phys.* **2017**, *147*, 164105.
- (41) Sokolov, A. Y.; Guo, S.; Ronca, E.; Chan, G. K.-L. *J. Chem. Phys.* **2017**, *146*, 244102.
- (42) Levine, B. G.; Ko, C.; Quenneville, J.; Martínez, T. J. *Mol. Phys.* **2006**, *104*, 1039–1051.
- (43) Nikiforov, A.; Gamez, J. A.; Thiel, W.; Huix-Rotllant, M.; Filatov, M. *J. Chem. Phys.* **2014**, *141*, 124122.

Graphical TOC Entry

